MATERIALS CHEMISTRY FRONTIERS

RESEARCH ARTICLE

View Article Online
View Journal | View Issue

Cite this: *Mater. Chem. Front.*, 2022, **6**, 3382

Highly efficient thermally activated delayed fluorescence emitter based on the 5*H*-benzo[*d*]benzo[4,5]imidazo[1,2-*a*]imidazole donor†

Manish Mannulal Raikwar, Seung Chan Kim and Jun Yeob Lee *

Received 10th August 2022,
Accepted 19th September 2022

DOI: 10.1039/d2qm00806h

rsc.li/frontiers-materials

In this study, a donor–π-acceptor-type thermally activated delayed fluorescence (TADF) emitter (**BzITz**) was designed and synthesized using 5*H*-benzo[*d*]benzo[4,5]imidazo[1,2-*a*]imidazole as a fused rigid electron donor, and a benzonitrile merged triazine unit as an electron acceptor. The effects of the fused rigid donor unit on the photophysical and electroluminescence properties of the TADF emitter were thoroughly explored. Compared with a reported emitter based on carbazole in a previous study, photophysical analysis results showed that **BzITz** exhibited a relatively small singlet–triplet energy splitting, a short delayed fluorescence lifetime, and a high photoluminescence quantum yield. Consequently, an organic light-emitting diode fabricated using the **BzITz** emitter exhibited an improved device performance with an external quantum efficiency of 24.0%, a current efficiency of 49.4 cd A^{-1}, and a low-efficiency roll-off. These findings show that the use of fused rigid donors can play a critical role in the design of efficient TADF emitters.

Introduction

Compared with traditional display technologies, organic light-emitting diodes (OLEDs) offer unprecedented advantages such as high contrast, lightweight and ultrathin properties, flexibility, wide viewing angles, and low-cost device production. However, designing highly emissive and stable emitters for OLEDs remains a significant challenge.[1–7]

Ordinary fluorescent materials have been used extensively as conventional OLED emitters, but their device performance cannot exceed the theoretical maximum exciton utilization efficiency of 25% because the yielded ratio of singlet and triplet excitons is 1 : 3 under electrical excitation conditions.[8,9] Conversely, because phosphorescent materials exhibit a strong spin–orbit coupling effect, the internal quantum efficiency (IQE) of the organic electroluminescence (EL) of phosphorescent materials can theoretically reach 100%.[10,11] Although phosphorescent materials exhibit excellent EL characteristics with unitary IQE and significant external quantum efficiency (EQE), the use of precious rare-earth metals limits their practical applications.[5,12–17] Recently, the development of emitters through thermally activated delayed fluorescence (TADF) has attracted significant attention, and TADF materials are termed as third-generation OLED emitters.[18–21] These materials are regarded as being highly efficient since they can achieve 100% IQE using triplet excitons through triplet-to-singlet thermal upconversion from the lowest triplet excited state (T_1) to the lowest singlet excited state (S_1) *via* reverse intersystem crossing (RISC).[18–20,22–24] Luminescent materials with a small S_1–T_1 energy splitting (ΔE_{ST}) can be obtained through a specific molecular design that involves minimal overlap between the highest occupied molecular orbital (HOMO) and the lowest unoccupied molecular orbital (LUMO) because of spatial separation of the electron-donating and electron-withdrawing units, enabling the thermal upconversion of electrons from the triplet to singlet excited states *via* RISC.[25–29] Consequently, TADF materials are being explored intensively for next-generation OLEDs, to overcome current technical limitations such as the device lifetime and color purity. In recent years, many researchers have developed highly efficient TADF materials with enhanced device performances using diverse acceptor and donor moieties.[30,31]

Donor–π–acceptor structures with twisted geometries have been used extensively to develop TADF materials.[32,33] In this framework, donor and acceptor moieties play a key role in determining the TADF properties *via* management of the HOMO and LUMO, which affects important TADF parameters such as the photoluminescence quantum yield (PLQY), delayed fluorescence lifetime, and ΔE_{ST}.[18] Several donor and acceptor moieties have been demonstrated as efficient and RISC-enhancing

School of Chemical Engineering, Sungkyunkwan University, 2066 Seobu-ro, Jangan-gu, Suwon, Gyeonggi, 440-746, South Korea. E-mail: leej17@skku.edu; Fax: (+) 82-31-299-4716

† Electronic supplementary information (ESI) available. See DOI: https://doi.org/10.1039/d2qm00806h

building blocks of TADF emitters. However, the exploration of more donor and acceptor moieties is necessary to improve the device performance of TADF OLEDs. In particular, new donor moieties without carbazole units need to be investigated to expand the material-design platform of TADF emitters.

In this study, we designed and synthesized a high-performance TADF emitter with a simple molecular skeleton of donor–π-acceptor architecture. The synthesized TADF emitter, 2-(5*H*-benzo[*d*]benzo[4,5]imidazo[1,2-*a*]imidazol-5-yl)-5-(4,6-diphenyl-1,3,5-triazin-2-yl)benzonitrile (**BzITz**), comprises a fused rigid donor 5*H*-benzo[*d*]benzo[4,5]imidazo[1,2-*a*]imidazole (**BzI**) and a triazine acceptor. The effects of the **BzI** donor on the photophysical and electrochemical properties were studied in detail. The use of this fused rigid donor decreased ΔE_{ST}, shortened the delayed fluorescence lifetime, and improved the PLQY of the emitter. Furthermore, the potential of this TADF material in multilayered OLED devices was explored. The device demonstrated an excellent performance with an EQE of 24.0% and a low-efficiency roll-off compared with other reported carbazole-based TADF emitters.

Results and discussion

Design strategy and synthesis

Our study aims to examine the effects of the carbazole-free fused rigid donor moiety on the physiochemical and EL properties of the designed TADF emitter. The synthesized TADF emitter was **BzITz** with a 5*H*-benzo[*d*]benzo[4,5]imidazo[1,2-*a*]imidazole (**BzI**) donor. The **BzI** donor was chosen because it has a high triplet energy and a strong electron-donating character. It can alter the lowest singlet and triplet excited states, playing an important role in controlling the ΔE_{ST} and thus the TADF mechanism of the synthesized material. A benzonitrile linker was introduced between the donor and the triazine acceptor, not only to facilitate the RISC process but also to increase the HOMO and LUMO overlap for efficient emission. Scheme 1 illustrates the chemical structure of the emitter and its synthetic procedures. Intermediate **1** was synthesized according to the reported procedures with some modifications.[34] Intermediate **2** was synthesized according to the procedure reported in our previous study.[35] In a potassium phosphate-mediated N-arylation reaction, the above-mentioned intermediates **1** and **2** were reacted together to yield **BzITz**. The chemical structure of the emitter was confirmed through ^{1}H and ^{13}C nuclear magnetic resonance (NMR) spectroscopy and mass analysis. The emitter was purified *via* vacuum train sublimation before being assembled into an OLED device.

Theoretical calculations

To gain insight into the electronic structure, physical properties, and orbital distributions (HOMO and LUMO) of the target molecule, we performed theoretical calculations on the unconstrained geometry of **BzITz** using the global hybrid functional B3LYP and the 6-31G* basis set of the Gaussian 16 program. Fig. 1 shows the optimized geometries for **BzITz** and its HOMO/LUMO distributions. The dihedral angle between the **BzI** donor and the adjacent benzonitrile spacer was 54.6° because of the steric hindrance caused by the cyano group on the benzonitrile spacer. This is useful for separating HOMOs and LUMOs and for lowering the ΔE_{ST}. As shown in Fig. 1, the HOMO is mainly localized on the **BzI** donor, whereas the LUMO is primarily delocalized on the diphenyltriazine acceptor with a small contribution from the two peripheral phenyl rings on triazine, the bridged benzonitrile spacer, and the nitrogen atom of the **BzI** donor. The LUMO electron density appears to be relatively low on the peripheral phenyl rings of diphenyltriazine because the electron-withdrawing cyano group tends to pull the electron density over the benzonitrile spacer, where it is attached. The calculated HOMO–LUMO energy gap (E_g) was 3.26 eV, derived from the HOMO of −5.54 eV and the LUMO of −2.28 eV. A moderate HOMO level similar to that of carbazole was observed. Time-dependent density functional theory (DFT) computations were performed to calculate the energies of the S_1 and T_1 states. Because of the spatially partitioned HOMO and LUMO, **BzITz** is expected to have a minimal ΔE_{ST}. The energies for the S_1 and T_1 states were 2.82 and 2.58 eV, respectively, resulting in a ΔE_{ST} of 0.24 eV. These findings suggest that **BzITz** would trigger effective RISC for TADF emission.

Furthermore, the natural transition orbital (NTO) distributions for **BzITz** were calculated using the long-range corrected ωB97XD functional with the 6-31+G* basis set. Fig. S2 (ESI†), displays the highest occupied natural transition orbital (HONTO) and the lowest unoccupied natural transition orbital (LUNTO) for the singlet and triplet excited states. In the singlet excited state, the HONTO and LUNTO were extensively separated with slight overlap, indicating that the singlet emission can be interpreted as charge-transfer (CT) emission. On the other hand, as

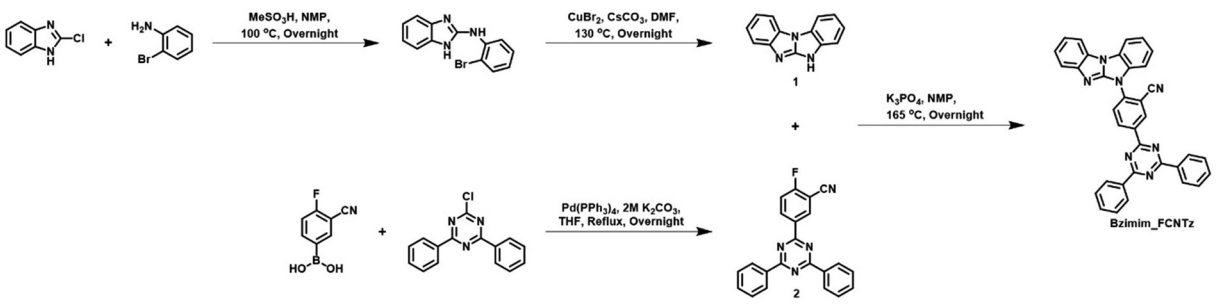

Scheme 1 Synthesis of the **BzITz** emitter.

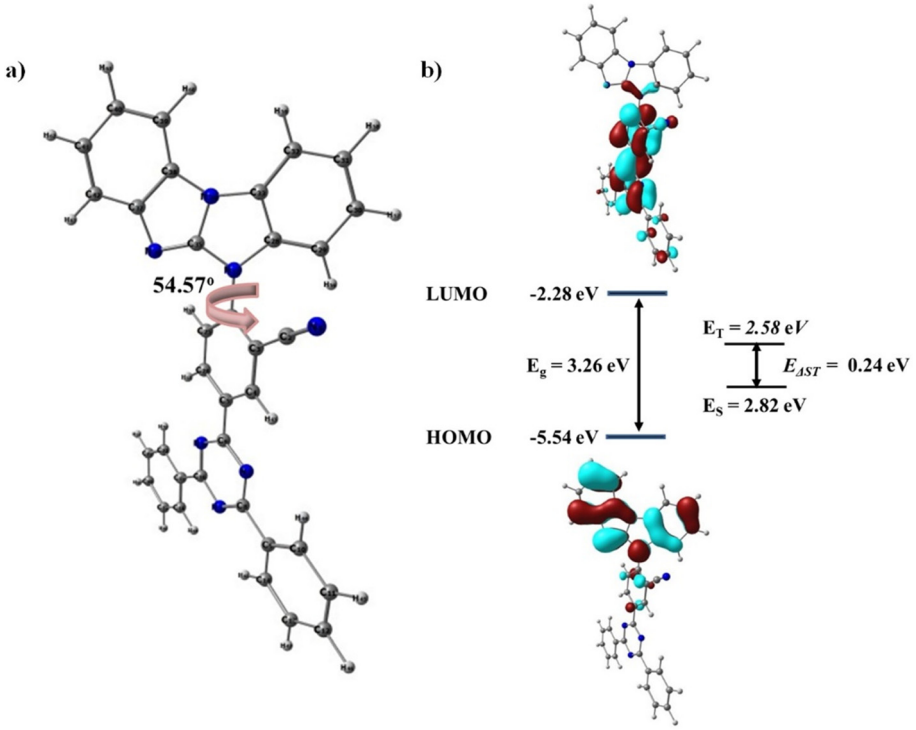

Fig. 1 (a) Optimized geometry and (b) frontier molecular orbital distributions of the compounds, estimated using the global hybrid functional B3LYP and the 6-31G* basis set on the Gaussian 16 program.

ascertained from the orbital pictures of the triplet excited state, the HONTO and LUNTO showed large overlapping over the phenyl ring of the benzonitrile unit and also separation, suggesting a mixed transition with CT and local-emission (LE) character. The mixed nature of the triplet excited state would be advantageous in increasing the RISC rate.[36]

Electrochemical properties

Cyclic voltammetry experiments were conducted on the emitter in dichloromethane using 0.1 M tetrabutylammonium perchlorate as the supporting electrolyte to investigate the emitter's redox characteristics. Oxidation potentials were calibrated using an Fc/Fc^+ redox couple, and Table 1 presents the results. With reference to ferrocene (Fc), the HOMO and LUMO energy levels of the emitter were determined from the onset potentials of the oxidation and reduction waves, respectively. The corresponding HOMO and LUMO energy levels for the emitter are −6.11 and −3.09 eV, respectively, and hence the resulting HOMO–LUMO gap is 3.02 eV. **BzI** demonstrated a robust donor character with a small oxidation potential because of the low electronegativity of nitrogen in **BzI**.

Photophysical properties

The optical properties of the emitter were measured through steady-state ultraviolet-visible (UV-vis) absorption and photoluminescence (PL) spectra. Fig. 2 shows the normalized absorption spectrum recorded in tetrahydrofuran (1.0×10^{-5} M) and the PL spectrum recorded in toluene (1.0×10^{-5} M) at room temperature (RT). The **BzITz** emitter exhibited two independent absorption bands in the range of 250–400 nm, where the short-wavelength band observed below ~300 nm is assigned to the localized π–π* electronic transitions of the aromatic segments, whereas the structureless broadband absorption at 365 nm is attributed to ICT from the **BzI** donor fragment to the diphenyltriazine acceptor fragment. The PL spectrum also exhibits single broadband emission at 461 nm, indicating that the singlet transition is initiated by CT states, as predicted by their spatially separated frontier molecular orbitals (Fig. 2). Furthermore, the emission profiles of the emitter were recorded in various solvents of varying polarity to better

Table 1 Photophysical and electrochemical data of the emitter

	λ_{abs}[a] (nm)	λ_{emi}[b] (nm)	E_S[c]/E_T[d] (eV)	ΔE_{ST}[e] (eV)	HOMO/LUMO[f] (eV)	E_g[g] (eV)	PLQY[h] (%)
BzITz	365, 274	461	3.05/2.88	0.17	−6.11/−3.09	3.02	98.8[i]/99.2[j]

[a] Measured in THF solution at RT. [b] Measured in toluene solution at RT. [c] Calculated from the onset of solid PL at RT. [d] Estimated from the onset value of phosphorescence spectra in toluene at 77 K. [e] Calculated singlet–triplet energy gap. [f] HOMO and LUMO estimated from cyclic voltammograms using HOMO = −(4.8 + E_{ox}); LUMO = HOMO − $E_{0\text{-}0}$. [g] Electrochemical bandgap obtained from the intersection of the absorption and emission spectra of THF solution. [h] Measured for 20 wt% doped films in DPEPO. [i] Under air. [j] Under nitrogen.

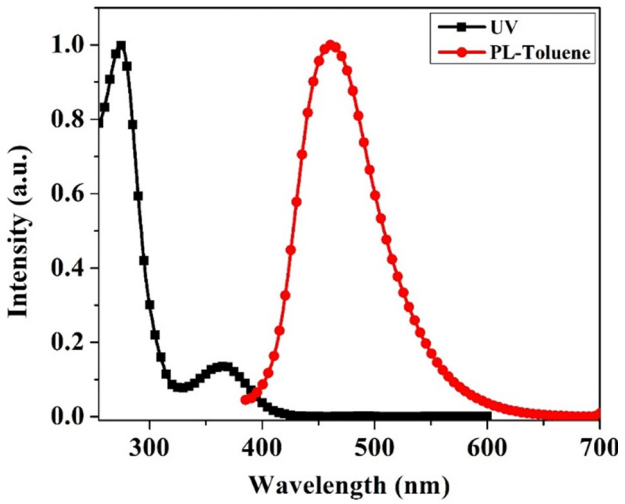

Fig. 2 Absorption spectrum (black) of the emitter recorded in THF solution and emission spectrum (red) recorded in toluene solution at RT.

understand the CT nature of the excited state (Fig. S1, ESI†). As the solvent polarity was increased from non-polar toluene (Tol) to polar tetrahydrofuran (THF), the emission spectrum of the emitter became gradually red-shifted. Generally, a red-shifted broad emission in polar solvents suggests CT-excited states of the emitter.[37] Therefore, **BzITz** can be regarded as a CT-based emitter.

The solid PL, low-temperature fluorescence (LTFL), and low-temperature phosphorescence (LTPL) spectra of **BzITz** were recorded at ambient temperature and at 77 K, respectively, to evaluate its light-emitting features, such as the S_1 and T_1 state energies. By doping with the emitter in a bis[2-(diphenylphosphino)phenyl]ether oxide (DPEPO) host at a concentration of 20 wt%, solid PL was measured (Fig. 3a). **BzITz** exhibited a broad CT emission in the blue region with a peak at 467 nm. The phosphorescence spectrum of the emitter was also broad, indicating that its lowest triplet state is a CT state (Fig. 3b).[38–41] The onset wavelengths from these LTFL and LTPL spectra were used to estimate the energy of the S_1 and T_1 states. The energies of S_1 and T_1 were 3.05 and 2.88 eV, respectively, providing a ΔE_{ST} of 0.17 eV. The emitter's small ΔE_{ST} value may efficiently promote T_1 to S_1 exciton upconversion through the RISC process.[19] The **BzI** donor generated a significant CT character in the emitter, lowering the singlet energy. Conversely, the triplet energy was maintained by the significant twisting between the donor and acceptor resulting from steric interactions between the cyano group on the benzonitrile spacer and the **BzI** donor. These results were consistent with the theoretical calculations.

Transient PL measurements of **BzITz** were conducted using 20 wt% emitter-doped films in a DPEPO host at RT in a vacuum to gain insight into the emitter's delayed fluorescence behavior. Fig. 4 shows the transient PL decay curve, and Table 2 provides the corresponding data. The emitter-doped film exhibited prompt and delayed components with lifetimes of 16.6 ns and 7.93 μs, respectively. The emitter's delayed fluorescence is attributed to the RISC process, where triplet excitons are thermally upconverted into singlet excitons. Furthermore, the PLQY values for the prompt (Φ_F) and delayed (Φ_{TADF}) components were calculated by measuring the absolute PLQY using an integrating sphere as 65.9% and 33.3%, respectively.[42] The total PLQY was 99.2% in a nitrogen atmosphere. The rate constants for prompt fluorescence (k_p), delayed fluorescence (k_d), intersystem crossing (ISC; k_{ISC}), RISC (k_{RISC}), and the radiative decay for singlet (k^S_r), and non-radiative decay (k^S_{nr}) were calculated,[43,44] and Table 2 presents the results. Because of the small ΔE_{ST}, the emitter had a lower k^S_{nr} value than k^S_r through an efficient upconversion process. The small ΔE_{ST} and low k^S_{nr} enhanced the PLQY of **BzITz**, implying that it has a substantial delayed-fluorescence contribution in light emission for use as a TADF emitter.

Electroluminescence properties

The EL performance of a vacuum-processed multilayer OLED device was investigated using **BzITz** as a dopant in the DPEPO host matrix. The OLED device configuration used was indium tin oxide (20 nm)/PEDOT:PSS (40 nm)/TAPC (10 nm)/mCP (10 nm)/EML (25 nm, 10 wt%)/TSPO1 (5 nm)/TPBi (20 nm)/LiF (1.5 nm)/Al (200 nm). To evaluate the doping-concentration effect, the doping concentration of **BzITz** was varied from 10% to 40%. Diphenylphosphine oxide-4-(triphenylsilyl)phenyl (TSPO1) and 1,3-bis(*N*-carbazolyl)benzene (mCP) were used as electron-transporting and

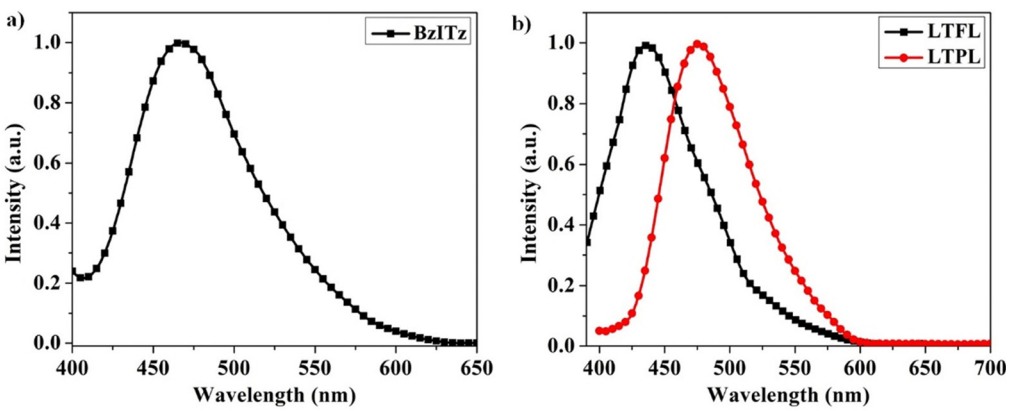

Fig. 3 (a) Emission spectrum of the emitter recorded in a 20 wt% doped DPEPO film, and (b) fluorescence (black) and phosphorescence (red) spectra of the emitter recorded in the THF matrix at 77 K.

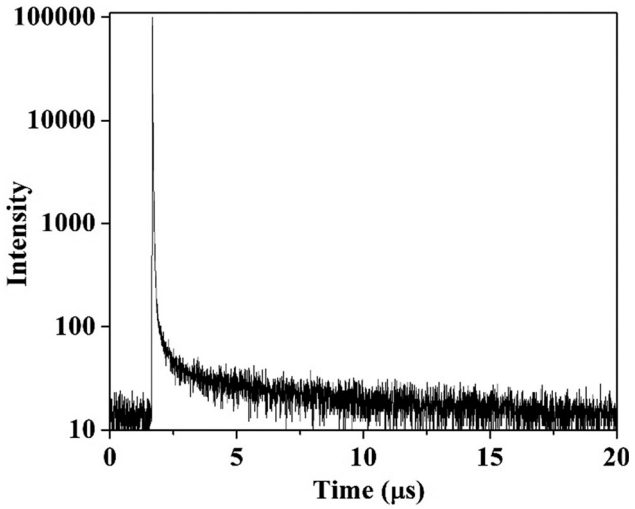

Fig. 4 Transient PL decay profiles of the 20 wt% emitter-doped DPEPO film.

hole-transporting exciton blocking layers, respectively. Di-[4-(*N*,*N*-ditolylamino)phenyl]cyclohexane (TAPC) and LiF were used as hole-transport and electron-injection layers, respectively. **BzITz**-doped (10, 20, 30, or 40 wt%) DPEPO layers were used as the emission layers. To maintain the excitons confined in the dopant, high-triplet-energy DPEPO was chosen as the host. Fig. 5 depicts the device structure, energy-level alignment diagram, and chemical structures of the organic materials used in the device. Fig. 6 shows current density–voltage–luminance, EQE–luminance, and EL plots of the **BzITz** devices. Table 3 summarizes the detailed device parameters.

As shown in Fig. 6a, the current density and luminance of the device gradually increase as the doping concentration is increased from 10% to 40%.[35,45–47] This is explained by the dopant-aided charge injection and hopping mechanisms. As the dopant has a deep LUMO and a shallow HOMO relative to the DPEPO host, direct charge trapping in the dopant would be the dominant EL process in these devices. The energy-level diagram shows that the significant HOMO gap between mCP and DPEPO disrupted the hole injection and transport. Consequently, the dopant plays a crucial role as a hole-trapping and -transporting medium in the device. Therefore, the current density and luminance of the **BzITz** devices increase with increasing doping concentration.[48]

Fig. 6b shows the EQE *vs.* *L* plots of the **BzITz** devices at various doping concentrations. The optimized device has a maximum EQE of 24.0% at a doping concentration of 30 wt%. Notably, when the doping concentration was increased from 30% to 40%, the **BzITz** device did not show any substantial decrease in EQE, showing that the concentration quenching effect is insignificant in the **BzITz** emitter. In general, the distance between emitters causes the concentration quenching effect because the prospect of exciton collision and quenching increases with the doping concentration. However, it was not severe with **BzITz** because of its sterically hindered design, which reduced strong intermolecular interactions and hence minimized concentration quenching.[49] This is further indirectly supported by the weak redshift in the EL spectrum with the doping concentration. The high EQE can be attributed to the emitter's high PLQY and high upconversion efficiency, which are aided by a small ΔE_{ST} and short t_d. As upconversion efficiency is critical to the EQE of the device because of the large population of triplet excitons in the EL mechanism, **BzITz** attained a high EQE by ensuring the efficient upconversion of triplet excitons into the singlet state. As shown in Fig. 6c, the EL spectra of the **BzITz** devices exhibited sky-blue

Table 2 Transient PL quantum yields and rate constants of **BzITz**

t_p[a] (ns)	k_p[b] (10^7)	t_d[a] (μs)	k_d[b] (10^5)	Φ_F[c] (%)	Φ_{TADF}[d] (%)	k_{ISC}[ef] (10^7 s^{-1})	k_{RISC}[eg] (10^5 s^{-1})	k_r^s[eh] (10^7 s^{-1})	k_{nr}^s[ei] (10^5 s^{-1})
16.6	6.02	7.93	1.26	65.9	33.3	2.02	1.90	3.97	3.20

[a] Prompt (p) and delayed (d) fluorescence lifetime. [b] Rate constant for prompt and delayed fluorescence lifetime. [c] Prompt and [d] delayed PLQY measured in DPEPO (20% dopant) thin film and calculated from the total PLQY and the proportion of the integrated area of the individual components in the transient spectra to the total integrated area. [e] Calculated using the equations reported in the literature.[43] [f] Rate constant for ISC. [g] Rate constant for RISC. [h] Radiative decay rate constant for a singlet. [i] Non-radiative decay rate constant for a singlet.

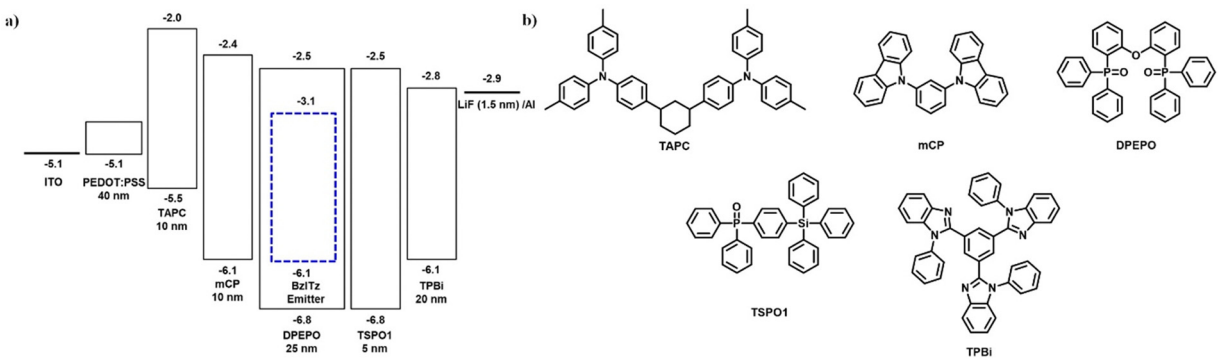

Fig. 5 (a) Device structure and energy-level alignment of the materials, and (b) chemical structure of the materials.

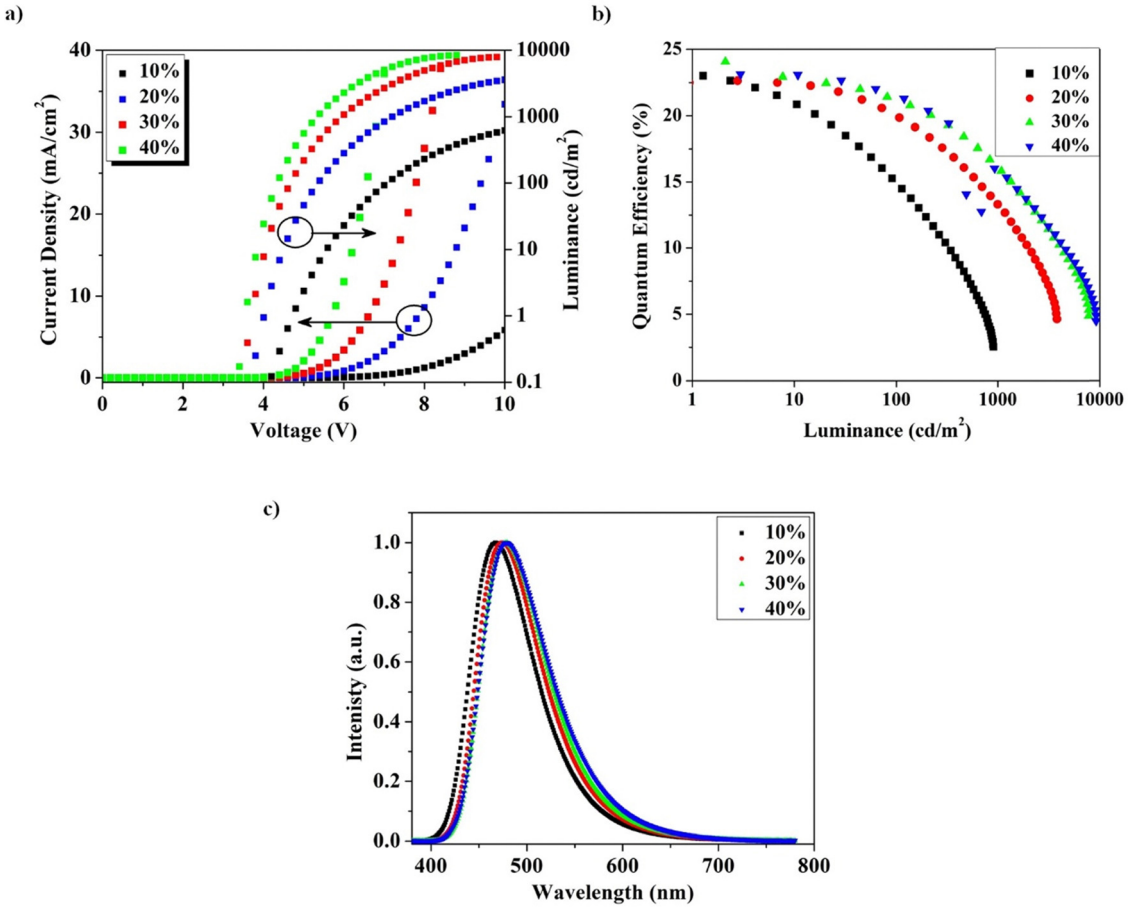

Fig. 6 (a) *J*–*V*–*L* plot, (b) EQE *vs.* luminance plot, and (c) EL spectra of the emitter.

Table 3 EL properties of the emitter

			EQE (%)		Current efficiency (cd A^{-1})		Power efficiency (lm W^{-1})		
Dopant	Concentration (wt%)	Voltage (V)	Max	@100 cd m^{-2}	Max	@100 cd m^{-2}	Max	@100 cd m^{-2}	CIE (x, y)
BzITz	10	9.4	23.0	15.0	37.7	24.1	27.9	10.7	0.17, 0.22
	20	6.5	22.6	20.0	43.4	37.7	35.7	22.1	0.17, 0.27
	30	5.4	24.0	21.2	49.4	43.1	40.8	29.1	0.18, 0.30
	40	5.2	23.1	21.7	41.4	32.6	50.1	46.6	0.19, 0.33

emission similar to the PL spectra with CIE color coordinates of (0.18, 0.30). In addition, the emitter exhibited a small redshift of ~12 nm when the doping concentration was increased from 10 to 40 wt% because of the use of a fused **BzI** donor. This small bathochromic shift observed in the EL spectra with an increasing doping concentration is attributed to strong intermolecular interactions at high doping ratios, which is common in host–guest-type OLEDs.[35,50] The devices did not produce any other emissions from the host material or any other layers, implying that energy was transferred efficiently from the host to the guest. Table 4 illustrates the comparison of the device performance for some previously reported non-rigid donors[35,51,52] and fused rigid donors[51–53] used in TADF emitters. In particular, compared with TADF emitters that have the same backbone structure, except for the donor, the EQE was significantly improved. Therefore, it can be concluded that the **BzITz** emitter showed promising device performance characteristics, indicating that such fused rigid donors can be used as potential donors for developing highly efficient TADF emitters.

Table 4 Comparison of EL properties of reported emitters

Emitter	EQE (%)	Ref.
TrzCz-CN	14.4	51
BFICNTrz, X = O	6.4	35
BTICNTrz, X = S	15.2	
BTITrz, X = S	20.7	52
BFITrz, X = O	12.0	
DICzCNTrz	21.4	53
CzDICzTrz	19.9	54

Conclusion

In summary, we have designed and synthesized a rigid **BzI**-donor-based sky-blue TADF emitter of **BzITz** with a diphenyltriazine acceptor and a benzonitrile spacer. The **BzITz** TADF emitter exhibited a small ΔE_{ST} of 0.16 eV and a high PLQY of 99.2%. According to the results, **BzITz** exhibited a high maximum EQE of 24.0% with a small concentration-quenching effect. Compared with the carbazole-derived donor, the **BzI** donor offered a high EQE because of its high PLQY, indicating that the fused rigid unit can be used as an effective donor for developing efficient TADF emitters.

Experimental section

All synthesis-related information is provided in the ESI.†

A device structure of indium tin oxide (20 nm)/PEDOT:PSS (40 nm)/TAPC (10 nm)/mCP (10 nm)/EML (25 nm, 10 wt%)/TSPO1 (5 nm)/TPBi (20 nm)/LiF (1.5 nm)/Al (200 nm) was used to test the TADF emitter. Vacuum deposition of the organic materials was used to form the thin film of organic materials at a vacuum pressure of 10^{-7} torr. Measurement of the electrical and optical performances of the devices was conducted using a Keithley 2400 source measurement and CS 2000 spectroradiometer system.

Conflicts of interest

There are no conflicts to declare.

Acknowledgements

This work was supported by MOTIE (20012556).

References

1 C. W. Tang and S. A. Vanslyke, Organic electroluminescent diodes, *Appl. Phys. Lett.*, 1987, **51**, 913–915.
2 J. H. Burroughes, D. D. C. Bradley, A. R. Brown, R. N. Marks, K. Mackay, R. H. Friend, P. L. Burns and A. B. Holmes, Light-emitting diodes based on conjugated polymers, *Nature*, 1990, **347**, 539–541.
3 J. R. Sheats, H. Antoniadis, M. Hueschen, W. Leonard, J. Miller, R. Moon, D. Roitman and A. Stocking, Organic electroluminescent devices, *Science*, 1996, **273**, 884–888.
4 H. J. Jang, J. Y. Lee, J. Kim, J. Kwak and J. H. Park, Progress of display performances: AR, VR, QLED, and OLED, *J. Inf. Disp.*, 2020, **21**, 1–9.
5 Z. Yang, Z. Mao, Z. Xie, Y. Zhang, S. Liu, J. Zhao, J. Xu, Z. Chi and M. P. Aldred, Recent advances in organic thermally activated delayed fluorescence materials, *Chem. Soc. Rev.*, 2017, **46**, 915–1016.
6 J. M. Teng, Y. F. Wang and C. F. Chen, Recent progress of narrowband TADF emitters and their applications in OLEDs, *J. Mater. Chem. C*, 2020, **8**, 11340–11353.
7 V. V. Patil, H. Lee, I. Kim, K. H. Lee, W. J. Chung, J. Kim, S. Park, H. Choi, W. J. Son and S. O. Jeon, Purely Spin-Vibronic Coupling Assisted Triplet to Singlet Up-Conversion for Real Deep Blue Organic Light-Emitting Diodes with Over 20% Efficiency and *y* Color Coordinate of 0.05, *Adv. Sci.*, 2021, **8**, 2101137.
8 L. J. Rothberg and A. J. Lovinger, Status of and prospects for organic electroluminescence, *J. Mater. Res.*, 1996, **11**, 3174–3187.
9 R. H. Friend, R. W. Gymer, A. B. Holmes, J. H. Burroughes, R. N. Marks, C. Taliani, D. D. C. Bradley, D. A. Dos Santos, J. L. Bredas, M. Logdlund and W. R. Salaneck, Electroluminescence in conjugated polymers, *Nature*, 1999, **397**, 121–128.
10 M. A. Baldo, D. F. O'Brien, D. Y. You, A. Shoustikov, S. Sibley, M. E. Thompson and S. R. Forrest, Highly efficient phosphorescent emission from organic electroluminescent devices, *Nature*, 1998, **395**, 151–154.
11 Y. X. Wang, J. H. Yun, L. Wang and J. Y. Lee, High Triplet Energy Hosts for Blue Organic Light-Emitting Diodes, *Adv. Funct. Mater.*, 2021, **31**, 2008332.
12 S. K. Jeon, H. Lee, K. S. Yook and J. Y. Lee, Recent Progress of the Lifetime of Organic Light-Emitting Diodes Based on Thermally Activated Delayed Fluorescent Material, *Adv. Mater.*, 2019, **31**, 1803524.
13 D. R. Lee, M. Kim, S. K. Jeon, S. H. Hwang, C. W. Lee and J. Y. Lee, Design strategy for 25% external quantum efficiency in green and blue thermally activated delayed fluorescent devices, *Adv. Mater.*, 2015, **27**, 5861–5867.
14 J. H. Kim, J. H. Yun and J. Y. Lee, Recent progress of highly efficient red and near-infrared thermally activated delayed fluorescent emitters, *Adv. Opt. Mater.*, 2018, **6**, 1800255.
15 M. Y. Wong and E. Zysman-Colman, Purely Organic Thermally Activated Delayed Fluorescence Materials for Organic Light-Emitting Diodes, *Adv. Mater.*, 2017, **29**, 1605444.
16 C. Li, R. S. Nobuyasu, Y. Wang, F. B. Dias, Z. Ren, M. R. Bryce and S. Yan, Solution-Processable Thermally Activated Delayed Fluorescence White OLEDs Based on Dual-Emission Polymers with Tunable Emission Colors and Aggregation-Enhanced Emission Properties, *Adv. Opt. Mater.*, 2017, **5**, 1700435.
17 X. Cai and S.-J. Su, Marching Toward Highly Efficient, Pure-Blue, and Stable Thermally Activated Delayed Fluorescent Organic Light-Emitting Diodes, *Adv. Funct. Mater.*, 2018, **28**, 1802558.
18 A. Endo, M. Ogasawara, A. Takahashi, D. Yokoyama, Y. Kato and C. Adachi, Thermally activated delayed fluorescence from Sn^{4+}-porphyrin complexes and their application to organic light-emitting diodes – A novel mechanism for electroluminescence, *Adv. Mater.*, 2009, **21**, 4802–4806.
19 H. Uoyama, K. Goushi, K. Shizu, H. Nomura and C. Adachi, Highly efficient organic light-emitting diodes from delayed fluorescence, *Nature*, 2012, **492**, 234–238.
20 Q. Zhang, B. Li, S. Huang, H. Nomura, H. Tanaka and C. Adachi, Efficient blue organic light-emitting diodes employing thermally activated delayed fluorescence, *Nat. Photonics*, 2014, **8**, 326–332.
21 H. J. Jang, J. Y. Lee, G. W. Baek, J. Kwak and J. H. Park, Progress in the development of the display performance of

AR, VR, QLED and OLED devices in recent years, *J. Inf. Disp*, 2022, **23**, 1–17.

22 B. D'Andrade, Applied physics: molecules that convert heat into light, *Nature*, 2012, **492**, 197.

23 Q. Zhang, J. Li, K. Shizu, S. Huang, S. Hirata, H. Miyazaki and C. Adachi, Design of efficient thermally activated delayed fluorescence materials for pure blue organic light emitting diodes, *J. Am. Chem. Soc.*, 2012, **134**, 14706–14709.

24 S. Y. Byeon, D. R. Lee, K. S. Yook and J. Y. Lee, Recent Progress of Singlet-Exciton-Harvesting Fluorescent Organic Light-Emitting Diodes by Energy Transfer Processes, *Adv. Mater.*, 2019, **31**, 1803714.

25 G. Mehes, H. Nomura, Q. Zhang, T. Nakagawa and C. Adachi, Enhanced Electroluminescence Efficiency in a Spiro-Acridine Derivative through Thermally Activated Delayed Fluorescence, *Angew. Chem., Int. Ed.*, 2012, **51**, 11311–11315.

26 J. Li, T. Nakagawa, J. MacDonald, Q. Zhang, H. Nomura, H. Miyazaki and C. Adachi, Highly Efficient Organic Light-Emitting Diode Based on a Hidden Thermally Activated, *Adv. Mater.*, 2013, **25**, 3319–3323.

27 H. Wang, L. Xie, Q. Peng, L. Meng, Y. Wang, Y. Yi and P. Wang, Novel thermally activated delayed fluorescence materials-thioxanthone derivatives and their applications for highly efficient OLEDs, *Adv. Mater.*, 2014, **26**, 5198–5204.

28 S. Y. Lee, T. Yasuda, Y. S. Yang, Q. Zhang and C. Adachi, Luminous butterflies: Efficient exciton harvesting by benzophenone derivatives for full-color delayed fluorescence OLEDs, *Angew. Chem., Int. Ed.*, 2014, **53**, 6402–6406.

29 S. Hirata, Y. Sakai, K. Masui, H. Tanaka, S. Y. Lee, H. Nomura, N. Nakamura, M. Yasumatsu, H. Nakanotani, Q. Zhang, K. Shizu, H. Miyazaki and C. Adachi, Highly efficient blue electroluminescence based on thermally activated delayed fluorescence, *Nat. Mater.*, 2015, **14**, 330–336.

30 S. H. Han, J. H. Jeong, J. W. Yoo and J. Y. Lee, Ideal blue thermally activated delayed fluorescence emission assisted by a thermally activated delayed fluorescence assistant dopant through a fast reverse intersystem crossing mediated cascade energy transfer process, *J. Mater. Chem. C*, 2019, **7**, 3082–3089.

31 K. M. Youn, H. Lee, H. J. Yoo, Y. H. Jung, J. Do Park, H. Jeong, J. Lee, J. Y. Lee and J. H. Kwon, High triplet energy bipolar host materials with the combination of dibenzofuran and benziimidazobenzoimidazole moieties for blue thermally activated delayed fluorescence emitter, *J. Mater. Chem. C*, 2020, **8**, 13811–13818.

32 M. Godumala, S. Choi, M. J. Cho and D. H. Choi, Thermally activated delayed fluorescence blue dopants and hosts: from the design strategy to organic light-emitting diode applications, *J. Mater. Chem. C*, 2016, **4**, 11355–11381.

33 D. H. Kim, K. Inada, L. Zhao, T. Komino, N. Matsumoto, J. C. Ribierre and C. Adachi, Organic light emitting diodes with horizontally oriented thermally activated delayed fluorescence emitters, *J. Mater. Chem. C*, 2017, **5**, 1216–1223.

34 W. Chung and J. Y. Lee, The role of the bulky blocking unit of the fluorescent emitter in efficient green hyper-fluorescent organic light-emitting diodes, *J. Inf. Disp.*, 2021, **22**, 49–54.

35 R. K. Konidena, K. H. Lee, J. Y. Lee and W. P. Hong, Triggering Thermally Activated Delayed Fluorescence by Managing the Heteroatom in Donor Scaffolds: Intriguing Photophysical and Electroluminescence Properties, *Chem. – Asian J.*, 2019, **14**, 2251–2258.

36 H. L. Lee, K. H. Lee, J. Y. Lee and H. J. Lee, Molecular design opening two emission pathways for high efficiency and long lifetime of thermally activated delayed fluorescent organic light-emitting diodes, *J. Mater. Chem. C*, 2021, **9**, 7328–7335.

37 R. K. Konidena, K. R. Justin Thomas, A. Pathak, D. K. Dubey, S. Sahoo and J.-H. Jou, Tuning the Photophysical and Electroluminescence Properties in Asymmetrically Tetra-substituted Bipolar Carbazoles by Functional Group Disposition, *ACS Appl. Mater. Interfaces*, 2018, **10**, 24013–24027.

38 D. R. Lee, S. H. Hwang, S. K. Jeon, C. W. Lee and J. Y. Lee, Benzofurocarbazole and benzothienocarbazole as donors for improved quantum efficiency in blue thermally activated delayed fluorescent devices, *Chem. Commun.*, 2015, **51**, 8105–8107.

39 L.-S. Cui, H. Nomura, Y. Geng, J. U. Kim, H. Nakanotani and C. Adachi, Controlling Singlet Triplet Energy Splitting for Deep-Blue Thermally Activated Delayed Fluorescence Emitters, *Angew. Chemie*, 2017, **129**, 1593–1597.

40 C. H. Ryoo, I. Cho, J. Han, J. H. Yang, J. E. Kwon, S. Kim, H. Jeong, C. Lee and S. Y. Park, Structure-Property Correlation in Luminescent Indolo[3,2-*b*]indole (IDID) Derivatives: Unraveling the Mechanism of High Efficiency Thermally Activated Delayed Fluorescence (TADF), *ACS Appl. Mater. Interfaces*, 2017, **9**, 41413–41420.

41 W. Huang, M. Einzinger, T. Zhu, H. S. Chae, S. Jeon, S. G. Ihn, M. Sim, S. Kim, M. Su, G. Teverovskiy, T. Wu, T. Van Voorhis, T. M. Swager, M. A. Baldo and S. L. Buchwald, Molecular Design of Deep Blue Thermally Activated Delayed Fluorescence Materials Employing a Homoconjugative Triptycene Scaffold and Dihedral Angle Tuning, *Chem. Mater.*, 2018, **30**, 1462–1466.

42 K. Masui, H. Nakanotani and C. Adachi, Analysis of exciton annihilation in high-efficiency sky-blue organic light-emitting diodes with thermally activated delayed fluorescence, *Org. Electron.*, 2013, **14**, 2721–2726.

43 G. H. Kim, R. Lampande, J. B. Im, J. M. Lee, J. Y. Lee and J. H. Kwon, Controlling the exciton lifetime of blue thermally activated delayed fluorescence emitters using a heteroatom-containing pyridoindole donor moiety, *Mater. Horiz.*, 2017, **4**, 619–624.

44 H. Noda, H. Nakanotani and C. Adachi, Excited state engineering for efficient reverse intersystem crossing, *Sci. Adv.*, 2018, **4**, 1–8.

45 T. B. Fleetham, L. Huang, K. Klimes, J. Brooks and J. Li, Tetradentate Pt(II) Complexes with 6-Membered Chelate Rings: A New Route for Stable and Efficient Blue Organic Light Emitting Diodes, *Chem. Mater.*, 2016, **28**, 3276–3282.

46 Y. J. Kang, J. H. Yun, S. H. Han and J. Y. Lee, Benzofuroacridine and benzothienoacridine as new donor moieties

for emission color management of thermally activated delayed fluorescent emitters, *J. Mater. Chem. C*, 2019, **7**, 4573–4580.

47 J. G. Yu, S. H. Han, H. L. Lee, W. P. Hong and J. Y. Lee, A novel molecular design employing a backbone freezing linker for improved efficiency, sharpened emission and long lifetime in thermally activated delayed fluorescence emitters, *J. Mater. Chem. C*, 2019, **7**, 2919–2926.

48 H. L. Lee, K. H. Lee, J. Y. Lee and W. P. Hong, Management of thermally activated delayed fluorescence using a secondary electron accepting unit in thermally activated delayed fluorescent emitters, *J. Mater. Chem. C*, 2019, **7**, 6465–6474.

49 X. Z. Xiao-Chun Fan, K. Wang, Y.-Z. Shi, D.-M. Sun, J.-X. Chen, F. Huang, H. Wang, J. Yu and C.-S. Lee, Thermally activated delayed fluorescence materials for nondoped organic light-emitting diodes with. nearly 100% exciton harvest, *SmartMat*, 2022, 1–11.

50 M. Kim, S. K. Jeon, S. H. Hwang and J. Y. Lee, Stable blue thermally activated delayed fluorescent organic light-emitting diodes with three times longer lifetime than phosphorescent organic light-emitting diodes, *Adv. Mater.*, 2015, **27**, 2515–2520.

51 H. Li, J. Li, D. Liu and Y. Mei, Mechanism evolution from normal fluorescence to thermally activated delayed fluorescence and color tuning over visible light range: Effect of intramolecular charge transfer strength, *Dyes Pigm.*, 2020, **183**, 108732.

52 R. K. Konidena, K. H. Lee and J. Y. Lee, 6*H*-Benzo[4,5]thieno[2,3-*b*] indole as a novel donor for efficient thermally activated delayed fluorescence emitters with EQEs over 20%, *J. Mater. Chem. C*, 2019, **7**, 13912–13919.

53 R. K. Konidena, K. H. Lee, J. Y. Lee and W. P. Hong, 15*H*-Diindolo[2,3-*b*1′,2′,3′-lm]carbazole: a novel rigid donor for highly efficient thermally activated delayed fluorescence emitters, *J. Mater. Chem. C*, 2019, **7**, 8037–8044.

54 R. K. Konidena, K. H. Lee and J. Y. Lee, Molecular design featuring carbazole-decorated 15*H*-diindolo[2,3-*b*:1′,2′,3′-lm] carbazole for improved efficiency and lifetime of thermally activated delayed fluorescence emitters, *J. Mater. Chem. C*, 2020, **8**, 2491–2499.

